Dear Author,

Please, note that changes made to the HTML content will be added to the article before publication, but are not reflected in this PDF.

Note also that this file should not be used for submitting corrections.

RSC Advances c5ra25451e

PAPER

1

An experimental and computational study to resolve the composition of dolomitic lime

J. Grant, G. L. Pesce, R. J. Ball, M. Molinari and S. C. Parker*

Dolomite phase separates during calcination suggesting enhanced properties of its mortars might be artificially produced by mixing fine powdered hydroxides.

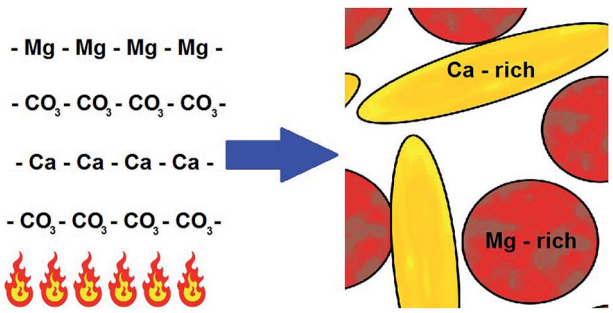

Please check this proof carefully. **Our staff will not read it in detail after you have submitted your proof corrections.**

Translation errors between word-processor files and typesetting systems can occur so the whole proof needs to be read. Please pay particular attention to: tabulated material; equations; numerical data; figures and graphics; and references. If you have not already indicated the corresponding author(s) please mark their name(s) with an asterisk. Corrections at this stage should be minor and not involve extensive changes. Please do not directly edit the text within the PDF file or send a revised manuscript. All corrections must be submitted at the same time.

Please bear in mind that minor layout improvements, e.g. in line breaking, table widths and graphic placement, are routinely applied to the final version.

We will publish articles on the web as soon as possible after receiving your corrections; **no late corrections will be made.**

Please return your **final** corrections, where possible within **48 hours** of receipt following the instructions in the proof notification email.

Queries for the attention of the authors

Journal: RSC Advances

Paper: c5ra25451e

Title: An experimental and computational study to resolve the composition of dolomitic lime

Editor's queries are marked like this... 1, and for your convenience line numbers are inserted like this... 5

Please ensure that all queries are answered when returning your proof corrections so that publication of your article is not delayed.

Query Reference	Query	Remarks
1	For your information: You can cite this article before you receive notification of the page numbers by using the following format: (authors), RSC Adv., (year), DOI: 10.1039/c5ra25451e.	
2	Please carefully check the spelling of all author names. This is important for the correct indexing and future citation of your article. No late corrections can be made.	
3	Fig. 1 appears to be of low resolution and therefore appears rather blurred. Would you like to resupply the image at higher resolution (preferably as a TIF file at 600 dots per inch)?	
4	Ref. 5 and 16: Please provide the thesis type (*e.g.* MPhil, PhD).	
5	Ref. 19, 32 and 49: Please provide the page (or article) number(s).	
6	Ref. 45: Please provide the last name for the 2nd author.	

RSC Advances

PAPER

An experimental and computational study to resolve the composition of dolomitic lime

Cite this: DOI: 10.1039/c5ra25451e

J. Grant,[a] G. L. Pesce,[b] R. J. Ball,[b] M. Molinari[a] and S. C. Parker*[a]

Received 30th November 2015
Accepted 26th January 2016

DOI: 10.1039/c5ra25451e

www.rsc.org/advances

Lowering the environmental impact, and moving away from a reliance on cement based binders, is a key challenge of the construction industry. Dolomitic lime binders are produced at lower temperatures than cement, re-adsorb released CO_2 during strengthening, and are recognised for their superior permeability, flexibility and resilience. While dolomite consists of alternating layers of magnesium and calcium the distribution in dolomitic lime is not yet fully understood. Here we combine experimental and computational methods to confirm that dolomite phase separates into lime and periclase during thermal decomposition. Raman inactivity of decomposed dolomite agrees with XRD studies suggesting phase separation. Our results rule out the formation of mixed phase oxides and predict an upper bound for bulk and surface substitution defect concentrations. Transferred to study macroscopic models of lime mortars these findings indicate that only the pure phases need be considered and that for the construction industry superior artificial mortars should be obtained from mixing fine powders of pure magnesium and calcium hydroxide.

Introduction

Cement and concrete production accounts for 7% of the anthropogenic CO_2 production.[1] The main contributions to this come from the fuel source and the CO_2 released during the production of cement. In contrast dolomitic lime binders are produced between 900 and 1250 °C instead of 1450 °C, and unlike cements set *via* carbonation. In addition they are more durable,[2–4] more permeable to water,[5,6] reduce damp problems, are self-healing,[7] withstand small movements without cracking, and have mild antiseptic properties against moulds. The reduced cost of production, carbon recapture during setting and longer lifetimes mean lime mortars have the potential to replace cement and impact CO_2 levels in the short, medium and long term. Dolomitic lime mortars therefore offer an alternative to our continued reliance on cement-based materials in construction.

Historically lime is one of the oldest inorganic binders after clay and gypsum with finds in Turkey having been dated to about 12000BC.[8] Lime mortars were used by the Phoenicians, in Egypt and Greece, reaching a technological peak with the Romans. During the Renaissance, lime was widely used and new technical treatises were published with detailed descriptions of the production and use of lime. However in the 18th and 19th century English and French engineers and scientists such as Smeaton and Vicat contributed to the development of the first scientific knowledge on lime and a new hydraulic binder, cement.[9] The practical properties of cement, in particular fast setting times meant that use and knowledge of lime mortars again went into decline.

Lime is typically produced by decomposing limestone, $CaCO_3$, into CaO releasing CO_2 but is also obtained from dolomite $CaMg(CO_3)_2$ which was known historically to enhance the properties of resulting mortars[10–12] and has recently been rediscovered.[13–16] Under mechanical testing medieval mosaics in St Mark's Basilica in Venice, bonded with dolomitic lime showed superior strength and durability.[13,17] Other researchers have also identified beneficial properties including lower porosity[18] and higher plasticity leading to better workability.[19] Before the mechanical and setting properties of the mortars can be studied we first need to identify the atomic structure of the initial mortar. Since the mortar is obtained from slaking calcinated dolomite it is reasonable to assume that the nature of the oxide mineral(s) will determine that of the mortar produced in thermal decomposition: if the oxides are phase-separated, the hydroxides in the mortar will be as well. Therefore an understanding of the decomposition products and thermodynamics of pure and mixed phase oxides and substitution defects is required.

Recent studies suggest that although the exact decomposition process of dolomite depends on the heating rate and conditions, it appears to decompose into phase-separated calcium and magnesium rich minerals.[20,21] Where decomposition appears to proceed in two stages, MgO first appears suggesting that it decomposes and migrates leaving $CaCO_3$ to decompose on longer timescales. One of the principle methods

[a]Department of Chemistry, University of Bath, Bath, UK. E-mail: S.C.Parker@bath.ac.uk

[b]Department of Architecture and Civil Engineering, University of Bath, Bath, UK

used to determine the decomposition products has been X-ray diffraction. While CaO, and/or $Ca(OH)_2$ and MgO have been identified in studies, researchers have not considered the potential properties of mixed phase oxides or defects in their analytic studies. There have been a number of theoretical studies of binary Ca–Mg systems of carbonate minerals. A number of these have investigated disordered mixed phase forms such as calcium-rich dolomite[22] and found them to be thermodynamically unstable, suggesting their existence is kinetic in origin.[22–25] In contrast dolomite is found to be stable in agreement with experiment, and Raman spectra have also been reproduced.[26] In the case of mixed phase oxides there is experimental evidence that these exist at high temperature[27] and as a result of molecular beam epitaxy.[28–30] Some theoretical work investigating thermodynamic stability has been reported at high pressure and temperature[31] and using the local density approximation (LDA).[32]

In this study we directly investigate the composition of dolomitic lime, confirming the degree of phase-separation and defect concentration following decomposition. This is essential to determining the relative properties of pure lime and dolomitic lime mortars. First, we compare experimental studies of carbonate minerals with simulation to validate the computational approach. We then consider the predicted properties of mixed-phase and minerals containing substitution defects in order to determine the constitution of decomposed dolomite.

Methodology

Samples and experiment

A reference sample of calcite was obtained from Jachymov, Czech Republic, magnesite was obtained from Brumado, Brazil. The dolomite reference was sourced from Bruch and der Mur, Austria while the decomposition sample was from a quarry near the city of Genoa, Italy. This stone has been used for production of lime mortars and plasters since the Middle Ages.[14,15] Samples were prepared by first crushing the stone with a hammer and then, the fragments obtained were finely powdered with a ceramic mortar and pestle. The resulting powder was sieved and particles between 60 and 125 μm were used for the decomposition process and the analyses.

All samples were decomposed using a thermo-balance SETARAM for TG/DTA analysis model TGA 92_1750 with a 1600 °C module. Tests were carried out on samples of 26.1 ± 0.1 mg using a dynamic regime, with a heating rate of 5 °C min^{-1} and a cooling rate of 20 °C min^{-1}. All tests were stopped at a temperature of about 80 °C in order to minimize water condensation on the sample particles and, thus, prevent carbonation while the samples were moved to a different laboratory for the subsequent analyses. During the decompositions, air gas was fluxed inside the furnace (internal pressure 150 kPa) in order to optimize the heat distribution and to promote the CO_2 removal from the crucible.

Raman spectra were acquired using a Renishaw inVia Raman Microscope. The system was equipped with lasers operating at wavelengths of 582 and 785 nm. The analyses were performed by focusing the laser with objective magnification 50×. Laser power was reduced to 50% whereas the acquisition time was set at 3 s for each of the 3 accumulations acquired. Each spectrum was taken over the wavenumber range 100–3200 cm^{-1}. Prior to the analysis, the spectrometer was calibrated using a monocrystalline silicon standard specimen. Peak fitting and deconvolution of Raman spectra was performed using Renishaw WiRe 4.0 software.

Models and computation

Our calculations have been performed VASP at the DFT level of description[33–36] using PBE exchange-correlation functionals[37,38] with a correction for van der Waals (vdW) forces, optB86b-vdW.[39,40] We studied single unit cells of carbonates, oxides (and elements) and 2 × 2 × 2 supercells of oxides using 4 × 4 × 1, 4 × 4 × 4 and 2 × 2 × 2 *k*-point meshes respectively, maintaining similar *k*-point densities. For the majority of the systems studied a plane wave cut off of 500 eV was sufficient though graphite required this to be increased to 800 eV to ensure convergence and stability of the optimised structure. Gases were studied with a single molecule in a 10 Å cubic box. Convergence for each system was ensured using electronic convergence criteria of 10^{-8} eV and ionic forces of 10^{-4} eV $Å^{-1}$, allowing atoms and lattice to relax. From the minimised structures vibrational frequencies were obtained using finite displacements.[41] Finally the Raman activity was obtained by calculating the polarizability for the vibrational modes.[42,43]

Initial configurations were obtained from experimental structures for the known minerals and are compared with the DFT optimised structures in Table 1. These show good agreement for both carbonates and oxides, all within 1.5% of experimental values.

We have considered three potential mixed phase configurations which are illustrated in Fig. 1 and compared with the mixed phase layered structure of dolomite. Dolomite is composed of alternating layers of calcium and magnesium; our study of mixed phase oxides considers alternating bilayers Fig. 1b and monolayers Fig. 1c in the {100} plane, alternating monolayers Fig. 1d in the {111} plane. Figures were generated with VESTA.[46] To complete the study we consider low concentration defects to approximate infinite dilution required for estimating the phase diagram with supercells containing 32

Table 1 Comparison of experimental and optimised lattice parameters for carbonate and oxide minerals. Lime and periclase are cubic so only a single value is given, while one in plane and the out of plane values are quoted for the trigonal carbonates

Mineral		Simulation (Å)	Experimental (Å)
Lime	*a*	4.79	4.8112 (ref. 44)
Periclase	*a*	4.23	4.2128 (ref. 44)
Calcite	*a*	5.03	4.9896
	c	16.80	17.0610 (ref. 45)
Magnesite	*a*	4.67	4.6328
	c	14.94	15.0129 (ref. 45)
Dolomite	*a*	4.84	4.812
	c	15.85	16.020 (ref. 45)

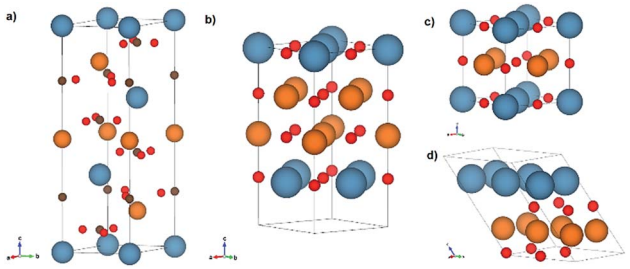

Fig. 1 Unit cells for (a) dolomite and (b–d) three candidate mixed phase oxides. Orange – magnesium, grey – calcium, green – carbon and red – oxygen. Dolomite is a layered structure, hexagonal in plane. Pure oxides are cubic: in (b) full unit cells each oxide are layered, (c) a single unit cell has single layers of each metal cation. In (d) the unit cell is reoriented such that the metal ions and oxygen are in separate layers {111} with alternating layers of magnesium and calcium.

formula units of CaO replacing one Ca with Mg, and *vice versa* (supercells of pure minerals were also simulated to allow for direct comparison of thermodynamic measurement).

Results

Before applying computational methods to determine the properties of mixed phase oxide structures it is useful to validate the computational method. To this end Fig. 2 compares Raman spectra obtained for three carbonate minerals, calcite, magnesite ($MgCO_3$) and dolomite, with simulated spectra. The calculated Raman intensities were fitted with Gaussians proportionate to the calculated activity. These predicted intensities are indicative; exact intensities and linewidths highly specific to the lasers and experimental conditions and require higher order calculations, for our current purposes the frequency and estimated activity suffice.

Fig. 2 shows that there is excellent agreement between the simulated and experimental spectra. Typically the location of peaks in spectra are not exactly reproduced. For instance in

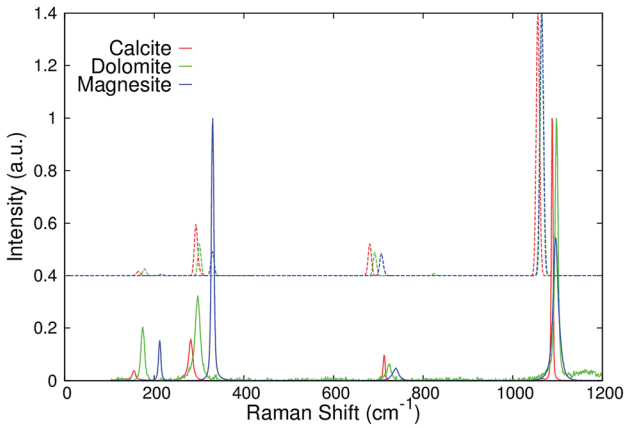

Fig. 2 Comparison of experimental (full lines) and simulated (dashed lines, offset) for carbonate minerals, calcite, dolomite and magnesite. Below 600 cm^{-1} there is excellent agreement between the simulated and experimental spectra. At higher frequencies a shift is observed but the order of peaks seen for the different minerals is reproduced.

Raman studies systematic shifts are often seen[43] due to error in the length and strength of bonds. This depends upon the functional used and while 'vibrational scaling factors' have been identified and routinely used, no correction has been applied in the data presented. Improvement in agreement can also be made by applying higher level methods, such as hybrid DFT/Hartree–Fock.[47] These have the further advantage that they can improve the accuracy of thermochemical quantities[48] but at a much increased computational cost. In spite of slight offsets the number, relative separation and order of peaks are consistent with experimental spectra. Data is not shown for lime and periclase because these minerals are not Raman active in either experiment or simulation.

The enthalpies of formation for the carbonate and oxide structures considered are given in Table 2. The minimised energies can be improved by including contributions to the free energy from vibrations identified in the finite displacement calculations using the harmonic approximation. Each mode contributes H_i, to the enthalpy of formation ΔH_f,

$$H_i = \frac{h\nu_i}{2} + h\nu_i\left(\exp\left(\frac{h\nu_i}{k_B T}\right) - 1\right)^{-1}$$

where h is Planck's constant, ν_i is the frequency of the mode, T the temperature and k_B Boltzmann's constant. Calculations were performed for the elements in order to estimate formation energies for the mineral, in the case of gases, oxygen and hydrogen contribution from rotations (k_BT) and translations ($3/2k_BT$) as well as work on the atmosphere (k_BT). The calculated enthalpies of formation show good agreement with experimental values, with all being within 6%. The formation enthalpies and Raman spectra validates the model for the systems.

The energy cost of the formation for the mixed phase, E_{mix}, relative to the pure mineral phases, is given by

$$E_{mix} = \Delta H_{mix} - n_A\Delta H_A - n_B\Delta H_B$$

where E_{mix} is the calculated energy, A and B are the pure minerals, ΔH_{mix} is the enthalpy of formation of the mixed phase or mixture, n_A is the number of formula units of A in the mixture (in the case of mixed phases $n_A = n_B = 0.5$) and ΔH_A is the enthalpy of a single formula unit of A. All values are for whole

Table 2 Comparison of calculated and experimental enthalpy of formation for pure and mixed phase carbonates and oxides. * Note that the experimental enthalpy quoted for dolomite is the enthalpy of mixing from calcite and magnesite

Model (Fig. 1)	Mineral	Calculated ΔH_f (kJ mol^{-1})	Experimental ΔH_f (kJ mol^{-1})	E_{mix} (kJ mol^{-1})
a	Calcite	−1159.4	−1207.6 (ref. 50)	—
	Magnesite	−1046.9	−1095.8 (ref. 50)	—
	Dolomite	−1105.9	−5.74* (ref. 49)	−2.8
	Lime (CaO)	−630.7	−634.9 (ref. 50)	—
	Periclase	−572.5	−601.6 (ref. 50)	—
b	Bi-{001}	−574.2	—	23.1
c	Mono-{001}	−566.2	—	31.1
d	Mono-{111}	−577.9	—	19.4

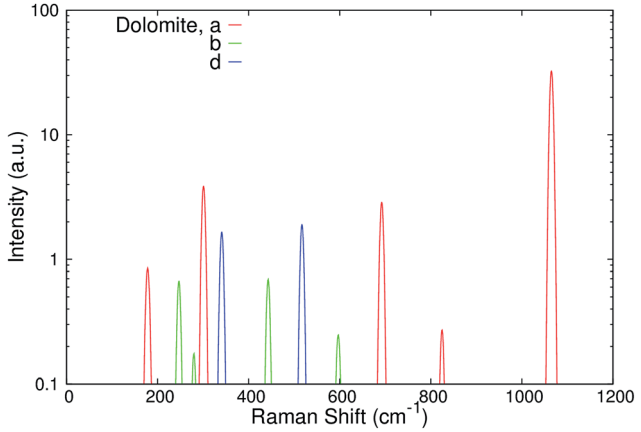

Fig. 3 Comparison of simulated Raman spectra for proposed mixed oxide structures and dolomite. The peak at ~200 cm^{-1} in the dolomite spectra is observed in experiment and since the spectra for the proposed mixed phase oxides have predicted Raman signals of a similar order we would expect the structures to be identifiable experimentally.

unit cells with carbonate minerals having 6 formula units per hexagonal cell and the oxides typically 4 (the exception is b) which has 8 formula units, the energy has been scaled for this system to allow easier comparison with the other mixed phase oxides. The calculations predict that dolomite is stable with respect to calcite and magnesite. The calculated formation energy for the dolomite unit cell is −2.8 kJ mol^{-1} compared with the experimental value of −5.75 ± 0.25 kJ mol^{-1} (ref. 49) at 85 °C. While the discrepancy appears large assuming error ~5 meV per atom in our calculations, corresponds to 2.5 kJ mol^{-1} for the carbonate minerals. Conversely the pure oxide minerals are significantly favoured, over all of the proposed mixed phase configurations.

The Raman spectrum for the mixed phase oxides shown in Fig. 3 provides further evidence that these mixed phases are not present in the experimental samples of decomposed dolomite. Two of the proposed structures are found to be Raman active in simulation having signals that are of the order of the predicted peak at ~200 cm^{-1} for dolomite which is seen in experiment. In contrast the decomposed dolomite was not Raman active consistent with the lack of activity in pure bulk lime[51] and periclase due to the inversion symmetry of the cubic crystal.[52] While structures (b) and (d) break the inversion symmetry (c) like the pure oxides is not Raman active, but has the highest predicted mixing energy of the candidate structures. This is consistent with physical intuition where we expect strain between different mineral layers the concentration of which is maximised in (c).

While we can be confident that phase-separation has occurred, we still expect some level of defect concentration as a result of entropic considerations. As a result, in the separated minerals, we would still expect disorder to result in some Raman activity due to the symmetry breaking from mixing metal ions. In order to estimate the concentration of defects we need to consider both the defect energy and entropy contributions to the free energy and their temperature dependence.

The simulation energies are the free energies at 300 K, both pure and defect calculations use supercells to avoid differences in the number of degrees of freedom and the impact this has on vibrational contributions to the free energy. Since contributions from vibrational modes are included using the harmonic approximation we take no account of volume change either from thermal expansion or the introduction of the defect and use the Helmholtz free energy. The contribution of each vibrational mode, A_i, is given by,

$$A_i = \frac{h\nu_i}{2} + k_B T \ln(1 - \exp(-h\nu_i/k_B T)).$$

The defect formation, or alternatively solution, energies ΔE_{def}, given in Table 3, are calculated similarly to the enthalpy of mixing of the mixed phases except that the free energy and number of formula units in the simulation cell are the relevant quantities. Values are quoted in eV to distinguish from the enthalpies of formation calculated previously and to highlight that these energies are estimates of low concentration defect energies that are independent of concentration. The free energy of solution at 300 K of calcium in periclase, 0.91 eV is more than magnesium in lime, 0.66 eV, due to the larger size of the calcium ion and therefore the greater strain associated with its substitution. As well as vibrational contributions to the Helmholtz energy we can consider the free energy difference between pure and defect systems due to entropy introduced by the defect. This can be estimated by an ideal, configurational, entropy of mixing per formula unit, ΔS_{id} given by

$$\Delta S_{id} = -k_B[x \ln(x) + (1 - x)\ln(1 - x)],$$

where x is the defect fraction per unit formula *e.g.* $Mg_xCa_{(1-x)}O$, and k_B, the Boltzmann constant in appropriate units. If the estimated free energy difference $\Delta A = \Delta E_{def} - T\Delta S_{id}$ is greater than 0 the system will phase separate, otherwise the defect concentration will be stabilised. We can therefore estimate the temperature at which particular defect concentrations are stabilised using

$$T_{bin}(x) = \frac{x\Delta E_{def}(T)}{\Delta S_{id}},$$

where $T_{bin}(x)$ is the temperature at which the phase boundary, the binodal, is located, where the defect energy has been normalised by the defect fraction to account for the defect being spread over $1/x$ formula units. Fig. 4 illustrates the estimated

Table 3 Simulation energies or pure minerals and defects 2 × 2 × 2 supercells of CaO, lime and MgO, periclase ignoring contributions from entropy of mixing. Defects replace one calcium ion with a magnesium, and *vice versa*

Mineral	n (CaO)	n (MgO)	A (300 K) (eV)	ΔE_{def} (300 K) (eV)
Lime	32	0	−361.48	—
Periclase	0	32	−313.96	—
Lime + defect	31	1	−359.34	0.66
Periclase + defect	1	31	−314.53	0.91

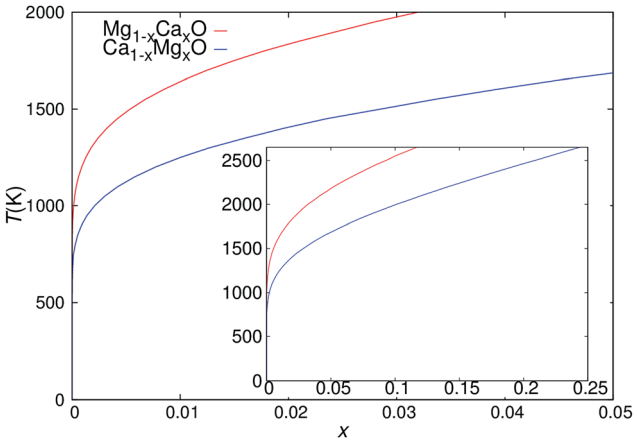

Fig. 4 Estimated phase diagram for low concentration solid solution as a function of x for $Ca_{(1-x)}Mg_xO$ and $Mg_{(1-x)}Ca_xO$ (inset: up to 25% defect concentration). Below the line phase-separation is favoured while above the lines the defect concentration will be stable.

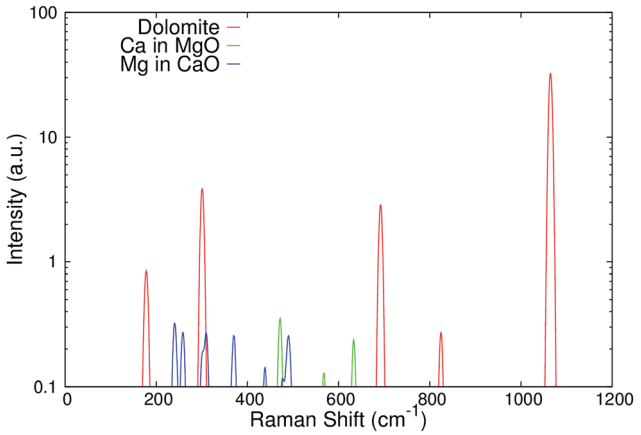

Fig. 5 Comparison of simulated Raman for dolomite, and supercells of MgO(CaO), containing a single Ca(Mg) defect. The spectra for the defect calculations are at a level that we would not expect to identify in experimental spectra. Since the simulated concentration defect corresponds to 3% stable bulk defect concentrations are predicted to be unobservable in Raman studies.

bulk phase diagram up to 2% defect concentration for the two systems considered. At these concentration we expect the defect free energy difference and entropy of mixing to be reasonable approximations. As the concentration is increased the mixing term breaks down because ordered structures have a lower mixing entropy, while the energy per defect is typically lowered when defects are adjacent. This is seen in the ordered mixed energies of the mixed-phase oxide structures, where the formation energies given Table 2 are typically smaller than the defect energies (since there are four formula units per unit cell there are two 'defects').

The predicted phase diagram is present in Fig. 4 showing the low concentration temperature dependence. In Fig. 4 (inset) concentrations are shown for temperatures up to 2650 K, above which liquid phases become important which cannot be captured by the present model. At standard conditions solid solutions are expected to be negligible. At temperatures up to 1500 K relevant to lime production solid solutions of 1% Mg in CaO and 3% are predicted, however unless the product is annealed rapidly equilibration at lower temperature will result in lower concentrations. At high temperature good agreement is observed between the predicted and experimental phase diagram for Mg in CaO. Experiment suggests solid solutions by mass of 17% at 2650 K and 10% at 2300 K, while we predict 19% and 12% respectively. These discrepancies could be due to a degree of equilibration during cooling, in both cases the experimental concentrations correspond to ~100 K lower than predicted, though this would be limited as the samples were annealed in water. At lower temperature the predicted phase diagram deviates significantly from experiment, but these samples were annealed in air which would allow longer for equilibration to occur during cooling.

While the predicted solid solutions for Ca in MgO are consistently lower they exceed the concentrations observed in experiment particularly at high temperature. That the discrepancy cannot be interpreted by equilibration during cooling alone suggests that the strain introduced due to the larger calcium ions is not captured as accurately as magnesium in lime. In both cases we note that the predictions are extremely sensitive to the calculated defect energies. As an illustration, an error of 50 meV, less than 10% of the free energy of solid solution corresponds to less than 1 meV per atom in the simulation cells studied. For Mg in CaO at 2000 K this equates to a 30% difference in the predicted concentration or equivalently a 150 K shift in the location of the binodal.

Simulated Raman spectra for the defect supercells are presented in Fig. 5, in comparison with that obtained for dolomite. The signals are typically comparable with the peak at ~800 cm^{-1} for dolomite which is not observed experimentally. The defect calculations show that at bulk concentrations of <3% the Raman signal is unlikely to seen experimentally consistent with the decomposed dolomite not being Raman active. While this concentration is greater than that predicted from the phase diagram it is useful to note that Raman is sensitive to the surface where defect concentration might differ substantially from the bulk. Previous studies have found enhanced defect concentration at surfaces where the strain introduced by the defect is reduced.[53] In the case of dolomite the experiment and simulation together suggest that any enhanced concentrations at surfaces must be at or below 3%.

Conclusions

We have analysed samples of dolomite supported by simulations of possible mixed-phase structures using a number of techniques to show that dolomite phase separates during decomposition. By applying computational and theoretical techniques we have also been able to show that any substitution defects are also likely to be of low bulk concentration. This result is of key importance in the development of both understanding the nature of dolomitic lime and the decomposition process. It will aid the production of new materials that are as

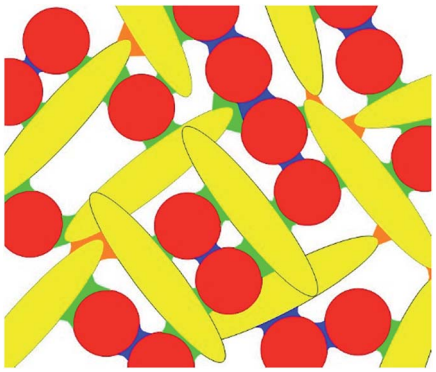

Fig. 6 Illustration of the microstructure of dolomitic lime. Calcium rich particles are shaded yellow, magnesium, red, morphologies are nominal but indicative of nanoparticles of hydroxylated minerals. Sintering between minerals is coloured differently to represent the different properties between different particle types.

practical as modern cements while retaining the beneficial properties of lime and dolomitic lime mortars.

Our calculations also predict that surface concentrations of defects are at most ~3%, since our current results predict these would not have detectable Raman signals. This is consistent with the decomposed dolomitic lime which was not Raman active. Enhanced defect concentrations at the surfaces are particularly important as these could have a disproportionate affect, since the surface structure will determine the rate of reactions. Therefore we would expect defects present to strongly influence the rate of hardening and strength of the resulting materials. As such, our results suggest it is the behaviour of pure minerals that determine the properties of lime mortars.

In Fig. 6 we give an illustration of the focus of current computational efforts to explain the properties of lime mortars. In dolomite calcium and magnesium rich particles will comprise the initial mortar (in calcic lime only calcium rich, portlandite particles, should be present). The strength and properties of sintering between particles will depend upon the atomic level carbonation, and the quality of the mineral deposited between the different particle types. The rate of carbonation will be determined by the delivery of carbon dioxide through the particulate system, and the removal of water. At the coarsest level the macroscopic properties will result from the interactions between phase-separated particles and qualities such as their elastic behaviour under strain. Further we predict that beneficial material properties for construction will be obtained by mixing current (calcium rich) lime stock with finely ground magnesium hydroxide powders.

Acknowledgements

The authors would like to thank the Engineering and Physical Sciences Research Council (EPSRC) for financial support through project EP/K025597/1. Access to ARCHER was provided *via* our membership of the Materials Chemistry Consortium, which is funded by EPSRC (EP/L000202). All data supporting this study are openly available from the University of Bath data archive at http://doi.org/10.15125/BATH-00170.

References

1 M. B. Ali, R. Saidur and M. S. Hossain, *Renewable Sustainable Energy Rev.*, 2011, **15**, 2252–2261.
2 G. C. Allen, *et al.*, *Hydraulic Lime Mortar for Stone, Brick and Block Masonry*, Donhead Publishing Ltd, Shaftesbury, Dorset, 2003.
3 I. Brocklebank, *Building limes in conservation*, Donhead Publishing, 2012.
4 J. J. Hughes and J. Valek, *Mortars in historic buildings: A review of the scientific and conservation literature*, Historic Scotland, 2003.
5 A. Forster, Heriot-Watt University, 2002.
6 J. Lanas and J. I. Alvarez-Galindo, *Cem. Concr. Res.*, 2003, **33**, 1867–1876.
7 D. Jaroenratanapirom and R. Sahamitmongkol, *J. Met., Mater. Miner.*, 2011, **21**, 9–17.
8 K. Kind-Barkauskas, B. Kauheen, S. Polonyi and J. Brandt, *Concrete Construction Manual*, Birkhauser, Basel, Switzerland, 2002.
9 P. C. Hewlett, *Lea's chemistry of cement and concrete*, Elsevier Butterworth-Heinmann, Oxford, 4th edn, 2004.
10 G. Misuraca, M. A. Bolidi and M. Aurelio, *L'arte moderna di fabbricare: trattato pratico ad uso degli ingegneri, costruttori, capimastri e studenti*, Milano, 1990.
11 T. Mannoni, *Fornaci da calce in provincia di Varese, Storia, conservazione e recupero*, Varese, 1995.
12 T. Mannoni, *Scienza e beni culturali*, Venezia, 2002.
13 G. C. Allen, *Journal of the Building Limes Forum*, 2008, **15**, 8–14.
14 D. T. Beruto, R. Vecchiattini and M. Giordani, *Thermochim. Acta*, 2003, **404**, 25–33.
15 D. T. Beruto, R. Vecchiattini and M. Giordani, *Thermochim. Acta*, 2003, **405**, 183–194.
16 R. Vecchiattini, University of Genoa, 2002.
17 R. Bertoncello, G. Biscontin, E. Croce, L. Milanese, L. Saragoni and E. Zendri, *Proceedings of the international conference Scienza e Beni Culturali*, 2002, vol. XVIII.
18 A. Arizzi and G. Cultrone, *Cem. Concr. Res.*, 2012, **42**, 818–826.
19 A. Arizzi, R. Hendrickx, G. Cultrone and K. ven Balen, *Mater. Constr.*, 2012, **62**.
20 C. Rodriguez-Navarro, K. Kudlacz and E. Ruiz-Agudo, *Am. Mineral.*, 2012, **97**, 38–51.
21 S. Gunasekaran and G. Anbalagan, *Bull. Mater. Sci.*, 2007, **30**, 339–344.
22 L. Chai, A. Navrotsky and R. J. Reeder, *Geochim. Cosmochim. Acta*, 1995, **59**, 939–944.
23 B. P. Burton and A. Van de Walle, *Phys. Chem. Miner.*, 2003, **30**, 88–97.
24 A. Zucchini, M. Prencipe, P. Comodi and F. Frondini, *CALPHAD: Comput. Coupling Phase Diagrams Thermochem.*, 2012, **38**, 177–184.

25 V. L. Vinograd, B. P. Burton, J. D. Gale, N. L. Allan and B. Winkler, *Geochim. Cosmochim. Acta*, 2007, **71**, 974–983.
26 J. Sun, Z. Wu, H. Cheng, Z. Zhang and R. L. Frost, *Spectrochim. Acta, Part A*, 2014, **117**, 158–162.
27 R. C. Doman, J. B. Barr, R. N. McNally and A. M. Alper, *J. Am. Ceram. Soc.*, 1963, **46**, 313–316.
28 E. S. Hellman and E. H. Hartford, *Appl. Phys. Lett.*, 1994, **64**, 1341–1343.
29 J. Nishii, A. Ohtomo, M. Ikeda, Y. Yamada, K. Ohtani, H. Ohno and M. Kawasaki, *Appl. Surf. Sci.*, 2006, **252**, 2507–2511.
30 M. Hlad, L. Voss, B. P. Gila, C. R. Abernathy, S. J. Pearton and F. Ren, *Appl. Surf. Sci.*, 2006, **252**, 8010–8014.
31 A. Srivastava, M. Chauhan, R. K. Singh and R. Padegaonker, *Phys. Status Solidi B*, 2011, **248**, 1901–1907.
32 R. Miloua, F. Miloua, Z. Kebbab and N. Benramdane, *ISJAEE*, 2008, **6**.
33 G. Kresse and J. Furthmüller, *Phys. Rev. B: Condens. Matter Mater. Phys.*, 1996, **54**, 11169–11186.
34 G. Kresse and J. Hafner, *Phys. Rev. B: Condens. Matter Mater. Phys.*, 1993, **47**, 558–561.
35 G. Kresse and J. Hafner, *Phys. Rev. B: Condens. Matter Mater. Phys.*, 1994, **49**, 14251–14269.
36 G. Kresse and D. Joubert, *Phys. Rev. B: Condens. Matter Mater. Phys.*, 1999, **59**, 1758–1775.
37 J. P. Perdew, K. Burke and M. Ernzerhof, *Phys. Rev. Lett.*, 1996, **77**, 3865–3868.
38 J. P. Perdew, K. Burke and M. Ernzerhof, *Phys. Rev. Lett.*, 1997, **78**, 1396.
39 J. Klimeš, D. R. Bowler and A. Michaelides, *Phys. Rev. B: Condens. Matter Mater. Phys.*, 2011, **83**, 195131.
40 J. Klimeš, D. R. Bowler and A. Michaelides, *J. Phys.: Condens. Matter*, 2010, **22**, 022201.
41 X. Wu, D. Vanderbilt and D. R. Hamann, *Phys. Rev. B: Condens. Matter Mater. Phys.*, 2005, **72**, 035105.
42 A. Fonari and S. Stauffer, *vasp_raman.py*, 2013, http://github.com/raman-sc/VASP/.
43 D. Porezag and M. R. Pederson, *Phys. Rev. B: Condens. Matter Mater. Phys.*, 1996, **54**, 7830–7836.
44 D. K. Smith and H. R. Leider, *J. Appl. Crystallogr.*, 1968, **1**, 246–249.
45 H. M. Effenberger, K. and J. Zemann, *Z. Kristallogr.*, 1981, **156**, 223–243.
46 K. Momma and F. Izumi, *J. Appl. Crystallogr.*, 2011, **44**, 1272–1276.
47 L. Valenzano, Y. Noël, R. Orlando, C. M. Zicovich-Wilson, M. Ferrero and R. Dovesi, *Theor. Chem. Acc.*, 2007, **117**, 991–1000.
48 B. M. Wong, D. Lacina, I. M. B. Nielsen, J. Graetz and M. D. Allendorf, *J. Phys. Chem. C*, 2011, **115**, 7778–7786.
49 A. Navrotsky and C. Capobianco, *Am. Mineral.*, 1987, **72**.
50 *CRC Handbook of Chemistry and Physics*, accessed 12th November 2015.
51 T. Schmid and P. Dariz, *J. Raman Spectrosc.*, 2015, **46**, 141–146.
52 R. G. Schlecht and H. K. Böckelmann, *Phys. Rev. Lett.*, 1973, **31**, 930–932.
53 J. A. Purton, S. C. Parker and N. L. Allan, *Phys. Chem. Chem. Phys.*, 2013, **15**, 6219–6225.